Published in final edited form as:
Nano Lett. 2009 December ; 9(12): 3974–3979. doi:10.1021/nl9018726.

Chemical Fabrication of Heterometallic Nanogaps for Molecular Transport Junctions

Xiaodong Chen[†,§], **Sina Yeganeh**[†], **Lidong Qin**[†], **Shuzhou Li**[†], **Can Xue**[†,§], **Adam B. Braunschweig**[†], **George C. Schatz**[†,*], **Mark A. Ratner**[†,*], and **Chad A. Mirkin**[†,*]

[†]Department of Chemistry and International Institute for Nanotechnology, Northwestern University, 2145 Sheridan Road, Evanston, IL 60208

[§]School of Materials Science and Engineering, Nanyang Technological University, 50 Nanyang Avenue, Singapore, 639798

Abstract

We report a simple and reproducible method for fabricating heterometallic nanogaps, which are made of two different metal nanorods separated by a nanometer-sized gap. The method is based upon on-wire lithography, which is a chemically enabled technique used to synthesize a wide variety of nanowire-based structures (e.g., nanogaps and disk arrays). This method can be used to fabricate pairs of metallic electrodes, which exhibit distinct work functions and are separated by gaps as small as 2 nm. Furthermore, we demonstrate that a symmetric thiol-terminated molecule can be assembled into such heterometallic nanogaps to form molecular transport junctions (MTJs) that exhibit molecular diode behavior. Theoretical calculations demonstrate that the coupling strength between gold and sulfur (Au-S) is 2.5 times stronger than that of Pt-S. In addition, the structures form Raman hot spots in the gap, allowing the spectroscopic characterization of the molecules that make up the MTJs.

Molecular transport junctions (MTJs) are essential structures for developing the field of molecular electronics.[1-3] One of the major challenges in building MTJs is the development of reliable methods for fabricating nanogaps, nanostructures that have metal electrode pairs separated by a few nanometers that enable electrical contact to targeted molecules. To date, five approaches have been evaluated for making nanogaps: (1) the mechanical break junction technique,[4,5] which is based on the mechanical breaking of a metal wire into two electrodes with a gap; (2) electromigration,[6-8] which involves passing a large electrical current through a gold nanowire to cause the electromigration of gold atoms and eventual breaking of the nanowire; (3) local oxidative cutting of carbon nanotubes with an oxygen plasma and a lithographic mask;[9] (4) microscopic gap narrowing by electrodeposition of metal in the gap;[10-12] and (5) shadow mask evaporation, in which nanoobjects, such as carbon nanotubes, nanowires, and nanofilms, are used as masks to make nanogaps.[13-15] Although impressive advances in making and characterizing MTJs have been made based on these techniques,[3] there are still major obstacles and limitations. For example, mechanical break junction and electromigration techniques require an expensive e-beam writer to generate nanowire patterns on substrates, and the yields of working devices are extremely low (typically less than 5%).[16] Furthermore, techniques explored to date have focused primarily on the fabrication of symmetric nanogaps, where the two electrodes are made of the same metal. Approaches for making heterometallic nanogaps, where the two electrodes are made of different metals, are interesting and useful for the field of molecular electronics

[*]Corresponding authors chadnano@northwestern.edu (CAM) ratner@northwestern.edu (MAR) schatz@chem.northwestern.edu (GCS).

both from fundamental and technological standpoints. Such structures, in principle, would allow researchers to tune the work functions of the electrode materials to better match the HOMO and LUMO of the molecules inserted in the gap. In addition, they may be extremely useful in the area of orthogonal self-assembly where adsorbate molecules can selectively assemble across such structures in a highly oriented fashion based upon different functional groups which are selective for the two metals.[17] So far, only one method for fabricating heterometallic nanogaps has been reported, involving the electrodeposition of a second metal on a pre-existing lithographically defined electrode.[18] The methods for making heterometallic nanogaps that involve narrowing procedures with micrometer-sized electrodes are complicated, difficult to control, and often very low yielding. Therefore, the development of efficient and highly parallel methods for fabricating heterometallic nanogaps with tunable dimensions would be a major step forward for the field of molecular electronics.

Recently, we developed a chemistry-based nanofabrication technique, on-wire lithography (OWL),[19] to prepare a wide variety of nanowire-based structures (e.g., nanogaps and nanodisk arrays) with control over composition and morphology. The obtained structures have been used for prototyping nanostructured materials for use in molecular electronics,[20,21] surface enhanced Raman spectroscopy,[22,23] plasmonics,[24] and energy conversion studies.[25] OWL allows one to prepare gaps with feature size control down to 2 nm, and therefore it is ideal for creating testbeds for studying MTJs.[20] The method is high-throughput, provides control over electrode length and composition, and allows one to tailor the gap size to molecular dimensions. Herein, OWL is used to fabricate heterometallic nanogap structures in a massively parallel manner. The obtained heterometallic nanogaps are used to construct MTJs through the assembly of thiolated molecular wires across a gap formed between two electrodes made of Pt and Au, respectively.

As a proof-of-concept, we use OWL to fabricate heterometallic nanogaps composed of platinum and gold. In a typical experiment, ~9 μm long, multisegmented Au-Ni-Pt-Au-Ni nanowires (diameter ~360 nm) were synthesized by sequential electrochemical deposition of gold (~3 μm), nickel (~10 μm), platinum (~2 μm), gold (~3 μm), and nickel (~1 μm) into AAO templates (Anodisc 47, Whatman).[26] (Note: a dash denotes the physical connection between segments, while an underscore (used later) indicates a gap between the segments.) The length of each segment can be controlled by monitoring the charge passed during the electrochemical deposition process (Figure 1a). The first nickel segment (10 nm) is a sacrificial layer, which can be removed subsequently to create a gap of well-defined thickness between the gold segment and the platinum segment by selective wet-chemical etching. The Ni segment thickness, and therefore gap size, is controlled by the number of coulombs passed in the electrochemical synthesis of the Ni layer. For instance, 3 nm Ni segments are obtained when 30 mC of charge is applied during electrochemical deposition, while 2 nm thick segments result from 20 mC of passed charge. The second Ni segment is used to demarcate the position of the platinum segment after the OWL process. The multisegmented nanowires are released from the template (Figure 1a) by removing the Ag backing layer in a solution of methanol, 30% ammonium hydroxide, and 30% hydrogen peroxide (4:1:1, v/v/v) and the dissolution of the AAO membrane in 3 M NaOH. By scanning electron microscopy (SEM) and energy-dispersive X-ray spectroscopy (EDS) experiments, one can see that a ~10 nm nickel segment is sandwiched between the gold and platinum segments (Figure 1 b and c). After the multisegmented nanowires were released from the template, they were dispersed on a glass substrate. A layer of silica (50 nm) was deposited on the nanowire-coated substrate by plasma-enhanced chemical vapor deposition (PECVD). Sonication releases the nanowires from the glass substrate and exposes the unprotected side of the nanowire. Dissolution of the nickel sacrificial layer with a HCl solution yields wires with heterometallic nanogaps whose dimensions can be precisely

controlled and where the electrode segments are fixed to an underlying silica coating. Significantly, SEM and EDS experiments clearly show that the nickel sacrificial layers have been removed, resulting in the formation of Au_Pt heterometallic nanogaps (Figure 1 d and e). In addition, we can make Au_Pt heterometallic nanogaps with smooth rod ends (Figure 1f) by an *in situ* two-step electrochemical process.[27]

This technique can be applied towards the fabrication of small heterometallic nanogaps (for instance, 3 nm and below what can be probed by EDS), which can be used in MTJ fabrication. In a typical experiment, 360 nm diameter wire structures with ~3 nm Au_Pt heterometallic nanogaps were cast onto a substrate with gold microelectrodes and then connected to the electrodes by e-beam lithography and subsequent chromium and gold thermal deposition (Figure 2a). The unmodified nanogap device was immersed in a tetrahydrofuran (THF) solution of α,ω-dithiol terminated oligo(phenylene ethynylene) (OPE, ~0.2 mg/mL) for 24 h, rinsed with THF, dichloromethane, and ethanol, and then blown dry with N_2. OPE was selected as a molecular wire because its length is appropriate to span the 3 nm gap defined by the OWL process, and the oligo(phenylene ethynylene) moiety is a well-known, conductive π-conjugated organic molecular wire from which a high quality monolayer can be prepared.[28]

The two terminal *I*-*V* characteristics of the ~3 nm gap devices were measured at room temperature (under vacuum (1×10^{-3} torr) in the absence of light) before and after molecular assembly. The empty nanogap exhibits no conductance within the noise limit of the measurement (< 2 pA). However, the nanogap devices loaded with OPE show a significant *I*–*V* response with rectifying behavior (black curve, Figure 2b), suggesting the assembly of the molecules across the gap with chemical connectivity to each of the metal electrodes on opposite sides of the gap. Importantly, only rods treated with the molecules have Raman spectra consistent with the OPE structure, and only these rods exhibit a rectification response. The rectifying behavior is likely a result of the different modes of contact between the ends of the molecules and the different electrode materials that span the heterometallic nanogap. One end of the molecule forms an Au-S connection while the other end forms a Pt-S connection (Figure 2c). These two different metal-molecule contacts induce different electronic coupling at the interface, different injection barriers, and unequal voltage drops. Furthermore, we deduce that hole transport from Au to Pt is enhanced leading to larger currents in the positive voltage regime than in negative bias where holes go from Pt to Au, and 30% of the OPE devices exhibited this rectification behavior. The remainder yielded no current above the noise limit of the measurement (~2 pA). Indeed, they exhibited current-voltage characteristics similar to the empty nanogap structures (indicating some failure in the construction of the junction). This success rate is significantly higher than that reported for other approaches.[16]

To analyze the asymmetric MTJ, we present a simple model based on the non-equilibrium Green's function technique.[29] We consider the single-level system in Figure 3, whose Green's function is given by

$$G^r(E)=[E-\varepsilon_0+i(\Gamma_L+\Gamma_R)]^{-1}, \quad (1)$$

where ε_0 is the single-level energy, and $\Gamma_{L,R}$ are the couplings of the molecule to the left/right electrodes. In the Landauer limit of elastic tunneling,[30] the current (*I*) can be written as a function of the applied voltage (*V*),

$$I(V)=\frac{2e}{\hbar}\int_{-\infty}^{\infty}\frac{dE}{2\pi}[f_L(E,V)-f_R(E,V)]|G^r(E)|^2\Gamma_L\Gamma_R, \quad (2)$$

where the Fermi functions are given by $f_k = [1 + e^{(E-\eta_k V)/k_B T}]^{-1}$. The η parameters describe the voltage drop across each interface, and we make the usual assumption that these are proportional to the couplings: $\eta_L = \Gamma_R/(\Gamma_L\,\Gamma_R)$ and $\eta_R = -\Gamma_L/(\Gamma_L + \Gamma_R)$. Thus, rectification originates from the asymmetric voltage drop across the interface due to different molecule-electrode couplings (see Figure 3). We use Eqn. 2 to fit to the experimental measurement and obtain Γ_{Au} = 23 meV, Γ_{Pt} = 9.4 meV, and ε_0 = 0.56 eV. Thus, we find that the Au-OPE coupling is roughly 2.5 times stronger than Pt-OPE, leading to the observed rectification.

SERS measurements directly on the nanogaps confirm that the OPE molecules assemble within Au_Pt heterometallic nanogaps. Sub-100 nm OWL-generated nanogaps have been shown to act as Raman “hot spots” with enhancement factors as large as 10^8[8,21,31] so molecules assembled within nanogaps can be identified spectroscopically by SERS measurements.[32,33] Theoretical calculations of extinction spectra of Au_Pt-Au gap structures reveal that adding a sub-50 nm long Pt segment does not affect the extinction spectra of the nanogap structures significantly (as compared with the homometallic Au_Au structure, Figure S2). This suggests the possibility of obtaining a SERS signal from molecules assembled within the nanoscale Au_Pt heterometallic gaps. Therefore, we synthesized Au (2 μm)-Ni (3 nm)-Pt (23 nm)-Au (2.4 μm) multisegmented nanowires (Figure 4a), which were then used to fabricate Au_Pt-Au heterometallic nanogaps using the procedure described above. The Au_Pt-Au heterometallic nanogaps were functionalized with OPE and subsequently characterized by confocal Raman and conventional bright-field microscopy (WiTec Alpha300). Samples were excited using a He-Ne laser (632.8 nm, Coherent Inc., Santa Clara, CA) with ~0.2 mW intensity. The confocal Raman images (Figure 4 b) were obtained by integrating the spectral intensity from 1500 to 1700 cm^{-1}, where 1593 cm^{-1} corresponds to the C-C ring stretch mode of OPE.[34] The observed SERS signal from the Au_Pt-Au heterometallic junction is comparable in intensity to the homometallic Au_Au junctions with a 3 nm gap size (Figure 4d).

To help interpret the SERS results, we have calculated electromagnetic fields for the heterometallic Au_Pt-Au nanogaps and the homometallic Au_Au nanogaps in vacuum using the discrete dipole approximation (DDA) method.[35,36] Here, only the light polarization parallel to the longitudinal axis of the wire nanostructure is considered since the coupling of the two plasmonic structures (such as for dimers in our previous work[23,37]) is most important for light polarized along this axis.[38] The grid spacing is 5 nm in all calculations and the gold dielectric constants are from Johnson and Christy.[39] As one example of such a calculation, Figure 5 presents the resulting SERS electromagnetic enhancement factor ($\int|E|^4 ds$) for the nanostructure as a function of location along the longitudinal axis of nanostructure, which is excited at 633 nm. For the two nanostructures considered in this figure, the Au segment length, Pt segment length, gap width, and diameter of the rod are 1000, 10, 10 and 360 nm, respectively. It was determined that the magnitude of the SERS enhancement factor at the gaps is larger than at the ends of the rods, which is in good agreement with our observed results (Figure 4). The peaks in the experiments are much broader than those in the calculations, as expected due to the lower spatial resolution and heterogeneity in the Raman microscopy experiments.

In summary, we have demonstrated a new method to chemically fabricate heterometallic nanogaps with tunable gap dimensions in a very high yield and in massively parallel fashion (approximately one billion of these dispersible heterometallic gap nanostructures are in one

experiment). Furthermore, this kind of heterometallic nanogap structure can be used for fabricating MTJs, which demonstrate rectification as a result of the different metallic interfaces available for chemical modification on opposite ends of the gap. In addition, the fabricated Au_Pt heterometallic nanogaps exhibit SERS enhancement behavior at the heterometallic junction, which can be used to spectroscopically identify molecules assembled within them. This method is complementary to inelastic electron tunneling spectroscopy, which has been used to study junctions fabricated by template-based nanowire device.[40,41] We anticipate that this new method of fabricating and characterizing MTJs based on heterometallic nanogaps will be used to create a wide variety of nanoelectronic devices with diverse functions and applications that derive from the types of metals used to make the electrodes and the molecules assembled with in them. Indeed, this initial work points towards the intriguing possibility of forming a bifunctional molecule capable of not only forming a MTJ within such heterometallic gap structures but also self-organizing and orienting within such structures based upon functional groups that direct the molecule ends to the corresponding electrode materials.

Supplementary Material

Refer to Web version on PubMed Central for supplementary material.

Acknowledgments

CAM is grateful for an NSSEF Fellowship from the Department of Defense and grant support from the DOE, DARPA, and NSF-MRSEC. XC thanks the support from NTU and NRF. ABB is grateful for an NIH Postdoctoral Fellowship (5F32CA136148-02). GCS and SL acknowledge the NSF-NSEC and DARPA. SY acknowledges the ONR for support through an NDSEG fellowship. MAR thanks the NSF Chemistry Division for support.

References

1. Lindsay SM, Ratner MA. Adv Mater. 2007; 19:23–31.
2. Nitzan A, Ratner MA. Science. 2003; 300:1384–1389. [PubMed: 12775831]
3. Tao NJ. Nat Nanotechnol. 2006; 1:173–181. [PubMed: 18654182]
4. Reed MA, Zhou C, Muller CJ, Burgin TP, Tour JM. Science. 1997; 278:252–254.
5. Reichert J, Ochs R, Beckmann D, Weber HB, Mayor M, von Lohneysen H. Phys Rev Lett. 2002; 88:176804. [PubMed: 12005775]
6. Park H, Lim AKL, Alivisatos AP, Park J, McEuen PL. Appl Phys Lett. 1999; 75:301–303.
7. Johnston DE, Strachan DR, Johnson ATC. Nano Lett. 2007; 7:2774–2777. [PubMed: 17696560]
8. Strachan DR, Smith DE, Johnston DE, Park TH, Therien MJ, Bonnell DA, Johnson AT. Appl Phys Lett. 2005; 86:043109.
9. Feldman AK, Steigerwald ML, Guo XF, Nuckolls C. Acc Chem Res. 2008; 41:1731–1741. [PubMed: 18798657]
10. Kashimura Y, Nakashima H, Furukawa K, Torimitsu K. Thin Solid Films. 2003; 438:317–321.
11. Qing Q, Chen F, Li PG, Tang WH, Wu ZY, Liu ZF. Angew Chem Int Ed. 2005; 44:7771–7775.
12. Xiang J, Liu B, Wu ST, Ren B, Yang FZ, Mao BW, Chow YL, Tian ZQ. Angew Chem Int Ed. 2005; 44:1265–1268.
13. Bezryadin A, Dekker C, Schmid G. Appl Phys Lett. 1997; 71:1273–1275.
14. Lefebvre J, Radosavljevic M, Johnson AT. Appl Phys Lett. 2000; 76:3828–3830.
15. Tang JY, Wang YL, Klare JE, Tulevski GS, Wind SJ, Nuckolls C. Angew Chem Int Ed. 2007; 46:3892–3895.
16. Qin LD, Jang JW, Huang L, Mirkin CA. Small. 2007; 3:86–90. [PubMed: 17294475]
17. Hickman JJ, Laibinis PE, Auerbach DI, Zou CF, Gardner TJ, Whitesides GM, Wrighton MS. Langmuir. 1992; 8:357–359.
18. Deshmukh MM, Prieto AL, Gu Q, Park H. Nano Lett. 2003; 3:1383–1385.

19. Qin LD, Park S, Huang L, Mirkin CA. Science. 2005; 309:113–115. [PubMed: 15994551]

(20). Chen XD, Jeon YM, Jang JW, Qin LD, Huo FW, Wei W, Mirkin CA. J Am Chem Soc. 2008; 130:8166–8168. [PubMed: 18528994]

21. Chen XD, Braunschweig AB, Wiester MJ, Yeganeh S, Ratner MA, Mirkin CA. Angew Chem Int Ed. 2009; 48:5178–5181.

22. Qin LD, Banholzer MJ, Millstone JE, Mirkin CA. Nano Lett. 2007; 7:3849–3853. [PubMed: 18041858]

23. Qin LD, Zou SL, Xue C, Atkinson A, Schatz GC, Mirkin CA. Proc Natl Acad Sci U S A. 2006; 103:13300–13303. [PubMed: 16938832]

24. Wei W, Li SZ, Millstone JE, Banholzer MJ, Chen XD, Xu XY, Schatz GC, Mirkin CA. Angew Chem Int Ed. 2009; 48:4210–4212.

25. Wei W, Li SZ, Qin LD, Xue C, Millstone JE, Xu XY, Schatz GC, Mirkin CA. Nano Lett. 2008; 8:3446–3449. [PubMed: 18767888]

26. Hurst SJ, Payne EK, Qin LD, Mirkin CA. Angew Chem Int Ed. 2006; 45:2672–2692.

27. Banholzer MJ, Li SZ, Ketter JB, Rozkiewicz DI, Schatz GC, Mirkin CA. J Phys Chem C. 2008; 112:15729–15734.

28. Tour JM. Acc Chem Res. 2000; 33:791–804. [PubMed: 11087316]

29. Yeganeh S, Galperin M, Ratner MA. J Am Chem Soc. 2007; 129:13313–13320. [PubMed: 17915864]

30. Meir Y, Wingreen NS. Phys Rev Lett. 1992; 68:2512–2515. [PubMed: 10045416]

31. Zheng GF, Qin LD, Mirkin CA. Angew Chem Int Ed. 2008; 47:1938–1941.

32. Tian JH, Liu B, Li XL, Yang ZL, Ren B, Wu ST, Tao NJ, Tian ZQ. J Am Chem Soc. 2006; 128:14748–14749. [PubMed: 17105252]

33. Ward DR, Halas NJ, Ciszek JW, Tour JM, Wu Y, Nordiander P, Natelson D. Nano Lett. 2008; 8:919–924. [PubMed: 18237152]

34. Richter LJ, Yang CSC, Wilson PT, Hacker CA, van Zee RD, Stapleton JJ, Allara DL. J Phys Chem B. 2004; 108:12547–12559.

35. Draine, BT.; Flatau, PJ. User guide to the Discrete Dipole Approximation Code DDSCAT 7.0. 2008. http://arxiv.org/abs/0809.0337v5

36. Kelly KL, Coronado E, Zhao LL, Schatz GC. J Phys Chem B. 2003; 107:668–677.

37. Chen XD, Li SZ, Xue C, Banholzer MJ, Schatz GC, Mirkin CA. ACS Nano. 2009; 3:87–92. [PubMed: 19206253]

38. Lassiter JB, Aizpurua J, Hernandez LI, Brandl DW, Romero I, Lal S, Hafner JH, Nordlander P, Halas NJ. Nano Lett. 2008; 8:1212–1218. [PubMed: 18345644]

39. Johnson PB, Christy RW. Phys Rev B. 1972; 6:4370–4379.

40. Mbindyo JKN, Mallouk TE, Mattzela JB, Kratochvilova I, Razavi B, Jackson TN, Mayer TS. J Am Chem Soc. 2002; 124:4020–4026. [PubMed: 11942840]

41. Cai LT, Skulason H, Kushmerick JG, Pollack SK, Naciri J, Shashidhar R, Allara DL, Mallouk TE, Mayer TS. J Phys Chem B. 2004; 108:2827–2832.

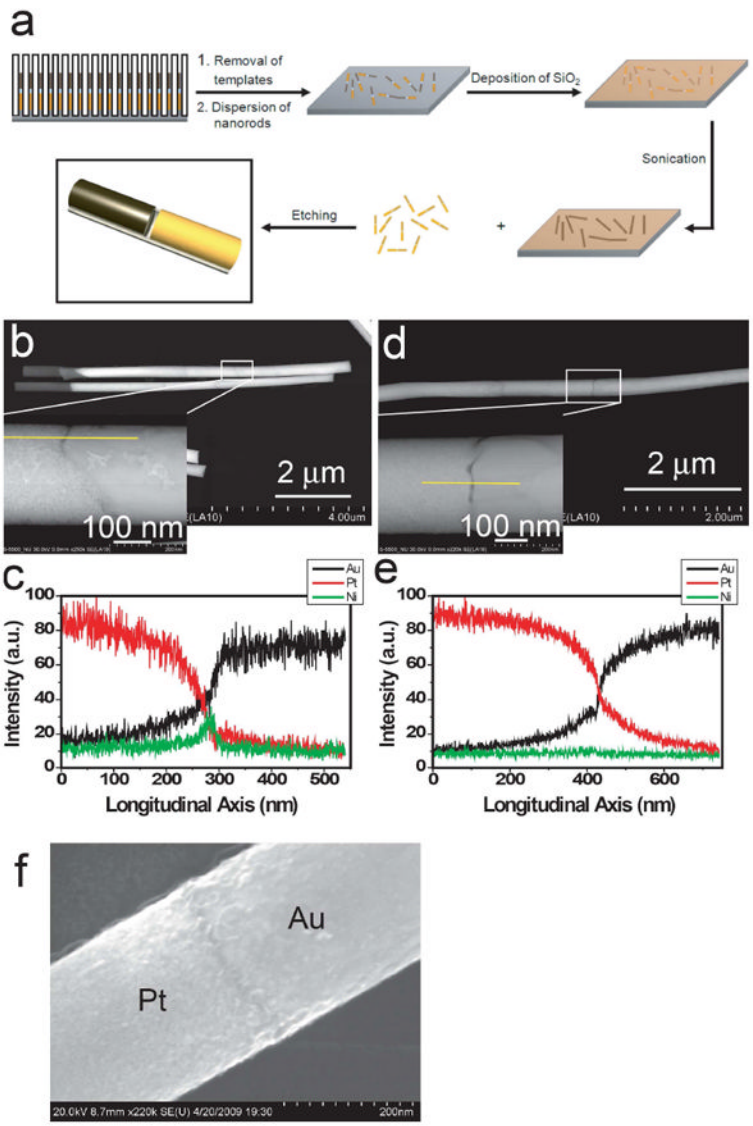

Figure 1.

(a) Scheme to prepare Au_Pt heterometallic nanogaps by OWL. SEM image of multisegmented nanowires before (b) and after (d) OWL. EDS line scan of a multisegmented nanowire before (c) and after (e) OWL. (f) SEM image of Au_Pt heterometallic nanogap with smooth rod ends.

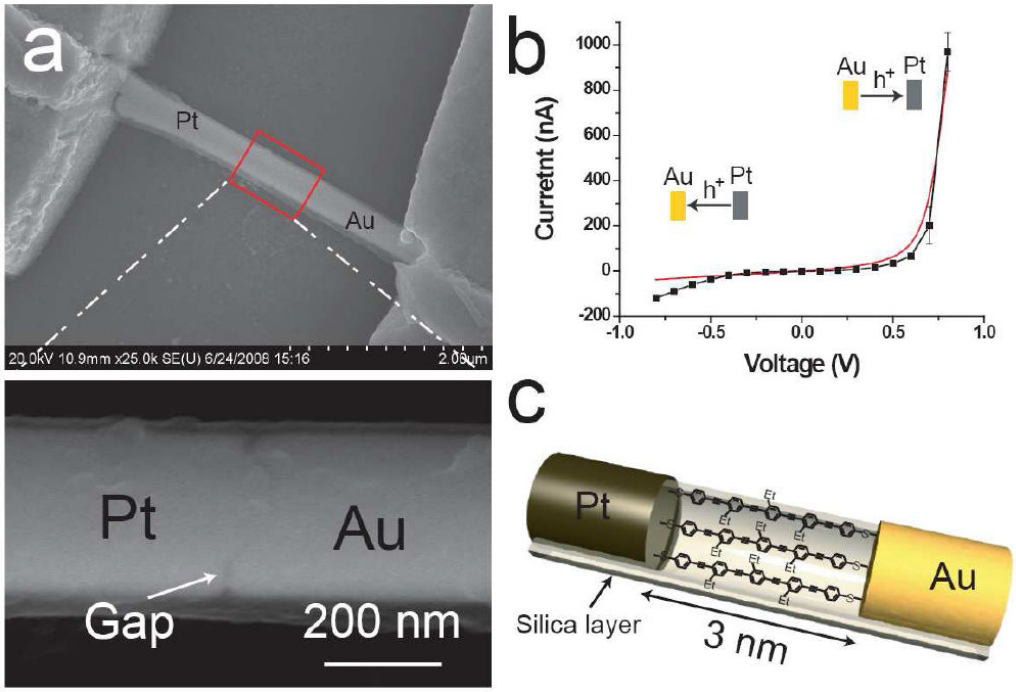

Figure 2.

(a) SEM image of an OWL-fabricated device with a ~3 nm Au_Pt heterometallic nanogap. (b) Representative *I-V* response for a ~3 nm OWL-fabricated heterometallic nanogap device modified with OPE. Theoretical fitted *I-V* curve (red curve). (c) A sketch of the device depicting the OPE molecules spanning the ~3 nm gap.

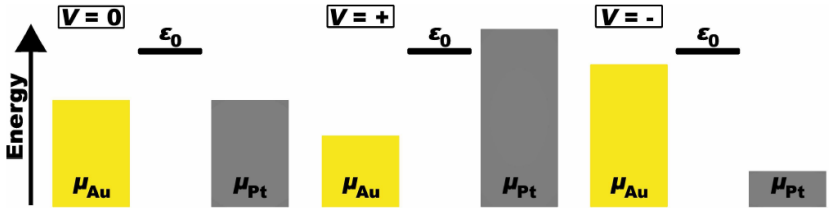

Figure 3.
The single-level model used for theoretical fitting is shown. At zero bias, the chemical potentials in both electrodes are nearly equal. When voltage is applied, however, the gold level will be more strongly pinned due to the larger Au-molecule coupling. This leads to resonant transport and higher current for positive voltage (increasing Pt chemical potential) and non-resonant transport and lower current for negative voltage (increasing Au chemical potential).

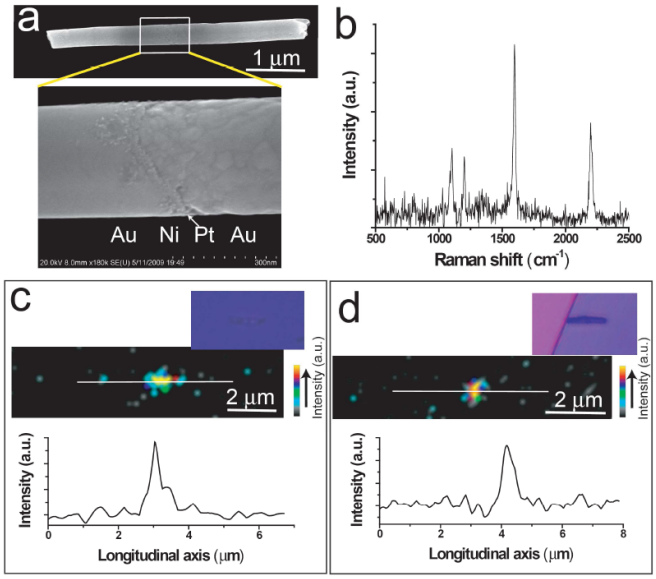

Figure 4.

(a) SEM image of an Au (2 μm)-Ni (3 nm)-Pt (23 nm)-Au (2.4 μm) multisegmented nanowire. (b) Representative Raman spectrum of OPE after assembly within a heterometallic Au_Pt nanogap structure. 2D confocal scanning Raman images and cross-section of the Raman intensity *vs* the location along the longitudinal axis (white line in c and d) of OPE modified (c) heterometallic Au_Pt nanogaps and (d) homometallic Au_Au nanogaps. Optical image (inset of c and d), which is simultaneously obtained, shows the orientation of the nanostructures.

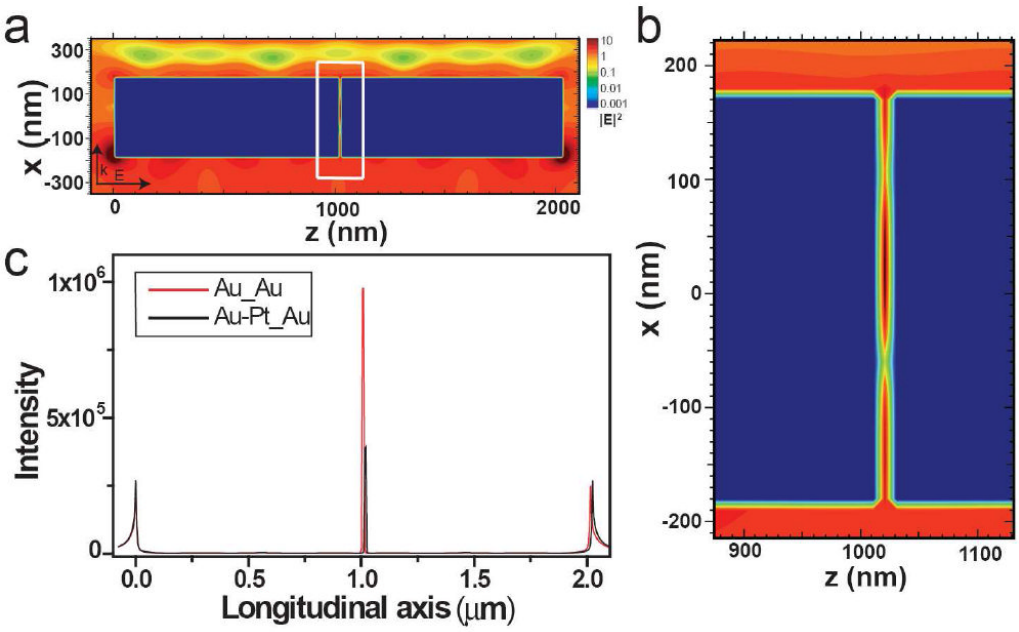

Figure 5.

(a) Electric field contour ($|E|^2$) of the Au-Pt_Au heterometallic nanogaps calculated with DDA in vacuum. (b) Enlarged contour for the Au-Pt_Au heterometallic nanogaps to clearly shows the electromagnetic hot spot at the junction. (c) The $\int|E|^4 ds$ intensity profile along the longitudinal axis is plotted for Au-Pt_Au heterometallic nanogaps (black curve) and Au_Au homo-nanogaps (red curve). The field enhancement is modeled for 633 nm radiation for the nanostructure with the following geometry: Au segment, 1 μm; Pt segment, 10 nm; gap width, 10 nm; diameter of rod, 360 nm; and grid spacing, 5 nm.